Photoionization of singly and doubly charged neon ions following inner-shell excitation

H. Yamaoka,[1,*] M. Oura,[1] K. Kawatsura,[2] T. Hayaishi,[3] T. Sekioka,[4] A. Agui,[5] A. Yoshigoe,[5] and F. Koike[6]
[1]*Harima Institute, RIKEN (The Institute of Physical and Chemical Research), 1-1-1 Kouto, Mikazuki, Sayo, Hyogo 679-5148, Japan*
[2]*Kyoto Institute of Technology, Matsugasaki, Sakyo, Kyoto 606-8585, Japan*
[3]*Institute of Applied Physics, University of Tsukuba, Tsukuba, Ibaraki 305-8573, Japan*
[4]*Faculty of Engineering, Himeji Institute of Technology, Himeji, Hyogo 671-2201, Japan*
[5]*Synchrotron Radiation Research Center, Japan Atomic Energy Research Institute (JAERI), 1-1-1 Kouto, Mikazuki, Sayo, Hyogo 679-5148, Japan*
[6]*Information Networking Center, Kitasato University, 1-15-1 Kitasato, Sagamihara, Kanagawa 228-8555, Japan*
(Received 11 September 2001; published 14 December 2001)

Photoion yields from Ne^+ to Ne^{2+} and from Ne^{2+} to Ne^{3+} were measured near the *K*-shell ($1s$-$2p$) autoionizing resonance region in the 841–858-eV and 850–863-eV photon energy range, respectively. Measurements were performed using a photon-ion merged-beam apparatus with an electron cyclotron resonance ion source. Multiconfiguration Dirac-Fock calculations were performed to interpret the experimental results. The calculations show fairly good agreement with the experimental results. Isonuclear series for the photoionization of Ne^+, Ne^{2+}, and Ne^{3+} are discussed.

DOI: 10.1103/PhysRevA.65.012709 PACS number(s): 32.80.Fb, 32.80.Dz

I. INTRODUCTION

Ionic structure and ionization processes are important subjects in atomic physics research and to understand nature, because ions are abundant in the cosmos, and information on the photoionization of ions is required for astrophysics, plasma physics, and the other fields. For example, $K\alpha$ lines of S, Ar, Ca, and Fe emitted from photoionized plasma were observed for highly charged ions such as hydrogenlike or heliumlike ions by the x-ray satellite ASCA [1,2]. However, due to the lack of experimental data for photoionization cross sections, for a long time theoretical values were used to interpret the observed data. Many efforts, mostly theoretical, have been made to obtain reliable photoionization cross sections, e.g., the Opacity Project [3] and the Iron Project [4,5].

During the past two decades, after the pioneering work by Lucatorto and McIlrath [6], photoionization experiments of ions have been performed in various laboratories [7–29,34]. But photoionization experiments are still difficult because it is hard to obtain a sufficiently high density ion target and at the same time a high flux photon beam. The ion density is normally much smaller than the target density of a neutral gas jet by five to six orders of magnitude and is comparable to that of the residual gas in an ultrahigh-vacuum (UHV) condition of the order of 10^{-8} Pa. To resolve these problems, the photon-ion merged-beam technique established by Dolder's group [8] has been used, with radiation from an insertion device or a bending magnet of a synchrotron light source.

Another method using the dual laser-produced plasma to investigate the inner-shell absorption spectra of ions has an advantage in that it can get photoabsorption spectra at the same time in a wide energy range with good energy resolution [20,21]. But the applicability seems to be limited when the incident photon energy goes from the soft-x-ray to the hard-x-ray region. Furthermore, measurement of the absolute cross section is difficult, the target species are limited, and analysis of the results is not simple because of the various phenomena happening in the plasma.

So far, the experimental data obtained for photoionization of ions are still limited. Experiments were carried out mostly for singly charged ions within a limited energy range. Therefore, extension of experimental work to almost every element ranging from helium to heavy ions in all ionization stages was desirable.

During the past decade, Koizumi's group has been performing photoionization experiments at the Photon Factory in KEK for Xe, Ba, Eu, Sr, and Cs ions by using the merged-beam method [22–28]. They measured photoion yields and studied spectral behavior around the $4d$ giant resonance region. The collapse of the $4f$ or $4d$ orbital was discussed by comparing the Z dependence. The targets were $4d$ or $3d$ electrons. Recently, they have made the absolute photoionization cross section measurements for Xe^+ ions [29]. To understand the experimental results, a multiconfiguration Dirac-Fock (MCDF) code such as GRASP has been used [30,31]. Recently, another theoretical approach has been developed by Tong *et al.* to understand the mechanisms of the giant resonance using density-functional theory with the optimized effective potential and self-interaction correction method [32,33].

Indeed, the third-generation synchrotron radiation sources, such as SPring-8, offer the opportunity to study the interaction of photons with inner-shell electrons, such as *K*-shell or *L*-shell electrons of ion targets, because of higher photon flux generated from soft to hard x rays by insertion devices installed in the storage ring. Thus we started a new project for photoionization experiments of ions at the SPring-8. The experiment is more difficult because, as the photon interaction with ions goes from outer shell to inner shell, the cross section becomes smaller. However these experiments are important not only for atomic inner-shell physics research but also for the fields mentioned previously.

*Email address: yamaoka@spring8.or.jp

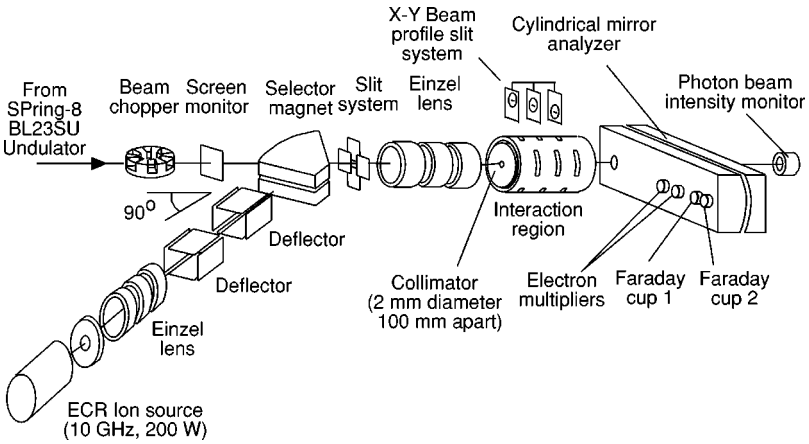

FIG. 1. Schematic diagram of the photon-ion merged-beam apparatus [35,36]. The apparatus mainly consists of an ECR ion source, a selector magnet, an interaction region, and an electrostatic analyzer. This was installed on the SPring-8 undulator beamline BL23SU [38].

The mapping of the resonance profiles along Q (isonuclear series for constant Z) or Z (isoelectronic series for constant Q), where Q is the number of electrons, provides the basic knowledge to understand the mechanism of the photoionization, the ionic structure, and the dynamics systematically. For example, isonuclear series provide information about many-body problems, and isoelectronic series provide information about the Z dependence of the relativistic or QED effect. In an isonuclear series, O'Sullivan *et al.* measured photoabsorption along iodine I, I^+, and I^{2+} [21], and recently Bizau *et al.* did the experiment for the single photoionization of Xe^{4+} to Xe^{7+} [19]. Koizumi *et al.* reported an interesting feature for the Z dependence of giant resonance about the doubly and triply charged photoion yield from singly charged Xe^+, Ba^+, and Eu^+ ions, although this is not an isoelectronic series [24].

In this paper, we present experimental results of the photoion yield measurements for singly and doubly charged neon ions in the region of the $1s$-$2p$ autoionizing resonance. Prior to these experiments, we performed a photoionization experiment from Ne^{3+} to Ne^{4+} [34]. Combining these results, we discuss the isonuclear system. In the experiment, a photoion merged-beam apparatus was used with an electron cyclotron resonance (ECR) ion source to produce a multiply charged ion target [35,36]. MCDF calculations were performed and compared to the experimental results.

II. EXPERIMENT

Figure 1 shows a schematic diagram of the experimental setup. The apparatus and the method have been described before [35,36]. Here a brief and additional description will be given. The apparatus consists of a compact ECR ion source, a selector magnet, an interaction region, and an electrostatic analyzer. The ions are produced by the 10 GHz, 200 W ECR ion source cooled by air. Gaseous or metal ions can be extracted by using this ion source. The advantage of using an ECR ion source was demonstrated by Bizau *et al.* for the photoionization experiment of highly charged Xe ions [19]. The typical operating rf power for neon ion production was only 5–10 W. The ions were then accelerated to 10 kV (the ion beam energy is $Q\times 10\,\mathrm{keV}$), and the beam was positioned before entering the selector magnet by the deflectors and the Einzel lens system. The magnet is a doubly focusing 90° sector magnet which can select the species for $1 \leqslant M/Q \leqslant 70$, where M is the atomic mass in the atomic mass unit.

The ions were directed into a 12-cm-long interaction region after refocusing by a second Einzel lens system, and collimation by a set of an adjustable slit system and a 2-mm-hole 100-mm-apart collimator. The interaction region was biased at a few kV to obtain the defined interaction length and to discriminate against the other stripped background signals generated outside the interaction region. The pressure in the interaction region was kept lower than 3×10^{-8} Pa to avoid collisionally induced ionization of primary ions with residual gas. In the interaction region, two sets of beam profile scanners were mounted, each consisting of a horizontal and a vertical three-slit system. Two-dimensional beam profiles were measured at three points along the beam direction.

After the interaction region, the ions were separated into different orbits according to the charge state of the ions so as to measure the primary ions by a Faraday cup and the photoionized ions by two electron multipliers. The cylindrical mirror analyzer (CMA) was biased electrostatically and the primary ions were doubly focused. The photoionized ions were detected by a single-particle detector, which consisted of a multiplier and a secondary electron converter plate in front of the electron multiplier cone. Two electron multipliers were mounted at the exit of the analyzer, but in these experiments we mainly used only one electron multiplier because of the low signal count rate of the doubly stripped product ions in the interaction region and the low signal-to-noise ratio. The background base pressure of the analyzer chamber was kept to less than about 6×10^{-8} Pa during the experiments.

The photon intensity was monitored by measuring the photoelectron current with a gold-plated photocathode at the end of analyzer chamber. The typical photoelectron current was 5.3 nA corresponding to a photon flux of the order of 10^{11} photons per second (in the low-resolution mode of the monochromator) [37]. A mechanical photon beam chopper in an UHV chamber was placed in front of the apparatus. The ion beam was chopped by applying a voltage to one of the deflectors. The measurement normally consists of four kinds of operation mode, which are a combination of on/off photon and on/off ion beams. In these experiments, we have per-

formed the measurements for two modes only, switching the photon beam on and off, because the background mainly originated from the noise presented when the ion beam was on. The noise without the ion beam was almost constant and negligibly small compared to the ion-beam noise, but by measuring this noise for a long period we took it into account to analyze the data when the ion beam was on. The data were taken for 20–30 sec at a given photon energy for each mode, with the photon beam on and off, respectively. All the data were normalized by the ion intensity, the photon beam intensity, and the measured time.

We add the fact that we performed the photoionization experiment for the Ne^{4+} beam, but the signal was under the detection limit in our experimental conditions, as will be described later. The ion-beam intensity, the signal count rate, and the background noise were typically 140 particle-nA, 70 and 10 000 cps for Ne^{+}, 45 particle-nA, 14 and 5000 cps for Ne^{2+}, 19–23 particle-nA, 15 and 2000 cps for Ne^{3+} [34], 3 particle-nA, no signal and 800 cps for Ne^{4+}, at maximum points, respectively, where particle-nA is the electric current divided by the ion charge. The noise was mainly due to the ion beam and roughly proportional to the ion-beam intensity. The background noise may originate through the process of charge exchange of the ion beam with residual gas, because the detectors can see the primary beam trajectory directly, thus the charge-exchanged ions can be accelerated toward the detectors according to the CMA bias potential. In the future, we may need to modify or change the analyzer system to reduce the background noise.

We measured the relative yield of the photoions as a function of the photon energy. To measure the absolute cross section, we need to measure the beam profiles of the photon and ion beams, and at the same time to confirm that the detector after the analyzer collects all product ions. In our experiments, the measurement of the absolute cross section was difficult because the real-time fine adjustments of the interaction region voltage to avoid the miscount of the product photoions were impossible due to the low signal-to-noise ratio.

On the other hand, the signal of photoions from the gaseous Ne target had enough intensity for the real-time adjustments. Therefore, the interaction region and analyzer voltages were set to the calculated values deduced from the experimental results of the photoionization of the gaseous Ne target, so that most of the product ions in the interaction region went to the electron multiplier position suitably. We used the beam profile slit system to confirm the overlap between the photon and the ion beams. Thus the ion beam was positioned to coincide with the photon beam by monitoring the beam profiles using the three *X*-*Y* beam profile slit system. The measured beam sizes (vertical×horizontal) of the photon and ion beams were typically 1.2×0.5 and $1.0\times1.2\,mm^2$ for Ne^{+}, 1.1×0.5 and $1.0\times1.2\,mm^2$ for Ne^{2+}, respectively.

The experiments were performed on BL23SU, a soft-x-ray undulator beamline, at the SPring-8, which employs a valid line spacing plane grating monochromator [38]. The apparatus was located about 110 m from the light source. The APPLE-2–type undulator can produce either linear or circularly polarized light [39]. During the experiments, the light was circularly polarized to reduce the heat load effect on the beamline optics. There was a refocusing mirror just before our apparatus and the photon beam was focused on the *x*-*y* slit position before the interaction region of the apparatus. We needed to repeat the same energy scan more than about several times to get meaningful data because the signal count rate was small and the statistical error due to the background was relatively large. The true signal was obtained by subtracting the counts when the photon beam was off and the average background when the photon and ion beams were off.

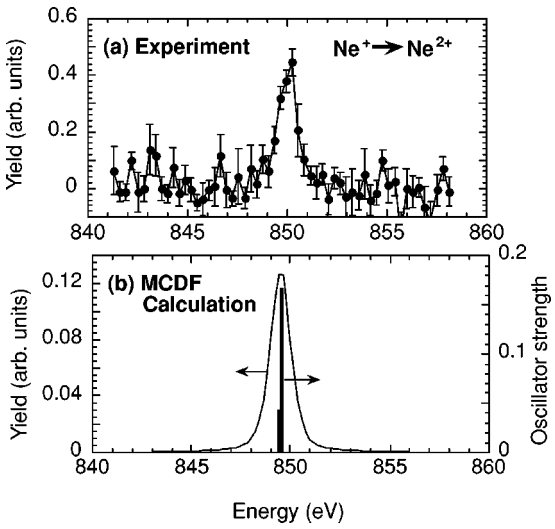

FIG. 2. (a) Relative photoion yield from Ne^{+} to Ne^{2+} with an energy resolution of $E/\delta E\sim670$ at the energy between 841 and 858 eV. (b) Calculated oscillator strength and convoluted spectrum with the system resolution. Statistical weights are multiplied for the calculated oscillator strength.

The energy scale of the monochromator was calibrated by measuring the total photoion yield of gaseous Ne and Xe. A small amount of Ne or Xe gas of about 10^{-4} Pa was introduced into the interaction region. Photoionized ions in the interaction region were accelerated by the bias potential. The measurement was performed with the high-resolution mode of the monochromator, $E/\delta E\sim6000$ at $E=867$ eV, where E is the photon energy. We used the energies of neon for $1s$-$3p$, 867.3 eV; $1s$-$4p$, 868.8 eV; and $1s$-$5p$, 869.5 eV, and those of Xe in the $3d$ threshold for the calibration, respectively [40,41]. The accuracy of the energy scale is ±0.2 eV. The photoionization experiments of the ion beams were performed with the low-resolution mode, $E/\delta E\sim670$ for Ne^{+} and Ne^{2+} and 770 for Ne^{3+}, to get higher photon flux.

III. RESULTS AND DISCUSSION

A. Ionization of singly charged neon ions

Figure 2(a) shows the experimental result of photoion yield measurement from Ne^{+} to Ne^{2+} in the 841–858-eV energy range, which corresponds to the region of $1s$-$2p$ autoionizing resonance. The error is about $\pm11\%$ at the maximum peak point. The spectrum is the sum of seven scans in

TABLE I. Initial states of $1s^22s^22p^5$, the total energy, and the higher-order energy correction for Ne^+. Higher-order energy correction includes the Breit interaction and the QED effect.

J	State	Total energy (eV)	Higher-order correction (eV)
$\frac{3}{2}$	$^2P_{3/2}$	−3481.78	0.713
$\frac{1}{2}$	$^2P_{1/2}$	−3481.69	0.705

the same energy range. The error mainly originates from the noise induced by the ion beam and the fluctuation of the ion-beam intensity during a few tens of seconds of the measurement at a given photon energy.

We made the MCDF calculations to assign the observed spectrum by using the GRASP[2], a revised version of the MCDF calculation code [31]. First, we evaluated the ground-state energy of Ne^+ ions including the configurations of $1s^22s^22p^5$ ($^2P_{3/2}$ and $^2P_{1/2}$) and other states. For the calculation of the ground state, we considered the atomic orbitals up to $4f$ to include effectively the electron correlation effects that are encountered through the two electron excitation configurations; using GRASP[2], we performed a configuration-interaction calculation after making an MCDF calculation with a minimal orbital set. The total energy of the initial states is summarized in Table I. Second, we calculated the excited states of Ne^+ ions including the configurations of $1s2s^22p^6$ ($^2S_{1/2}$), $1s2s^22p^53p$, and others to the $4f$ state. The photoexcitation energies were corrected by replacing the initial-state total energy obtained in the second step by the one obtained in the first [23]. As a result, the amount of energy correction was 5.276 eV for $^2P_{3/2}$ and 5.260 eV for $^2P_{1/2}$, respectively. Here we considered the higher-order correction including the Breit interaction (spin-spin interaction and spin-other electron orbital angular momentum interaction) and the QED effect (Lamb shift) for the MCDF calculation. Neon is a relatively light atom and these corrections are basically small. For the excited states, the same effects were considered, but the corrections were less than half the values of those in the case of the ground states. Normally, for the case of outer-shell or valence electrons, we can ignore the above correction when we take the energy difference between the ground state and the excited state. But in this case the $1s$ electron moves in the inner-shell strong field when the ionization occurs and thus the small energy difference of the order of 0.7 eV for the ground state still remains.

In Table II, the energy levels and the oscillator strengths are shown. In Fig. 2(b), the theoretical spectrum convoluted with the system resolution of $E/\delta E \sim 670$ by using a Voigt function is shown assuming the Lorentzian natural linewidth of 0.27 eV [40]. Here the statistical weights are multiplied for the oscillator strengths. The convoluted theoretical spectrum shown in Fig. 2(b), however, shows fairly good agreement with the experimental result, although the calculated energy scale should be shifted by about 0.5 eV to the higher-energy side. The calculation shows that the peak in Fig. 2(a) consists of two transitions, $^2P_{3/2} \rightarrow {}^2S_{1/2}$ and $^2P_{1/2} \rightarrow {}^2S_{1/2}$. The energies of these lines are close, therefore the observed peak was relatively sharp compared to the peaks for the photoionization of highly charged ions described later.

TABLE II. Calculated energy levels and oscillator strength for Ne^+.

Energy (eV)	Initial state $1s^22s^22p^5$	Excited state $1s2s^22p^6$	Oscillator strength
849.42	$^2P_{1/2}$	$^2S_{1/2}$	0.126
849.51	$^2P_{8/2}$	$^2S_{1/2}$	0.250

Single photoionization of neon ions occurs through the Auger process, and the fluorescence yield may be small as with neutral neon. We did not measure the doubly stripped ions, from Ne^+ to Ne^{3+}, due to the large background noise and the limitations of the present experimental conditions. The cross section of double photoionization will be smaller because Ne^{3+} ions will be produced through the double Auger process from the excited state of $1s2s^22p^6$. The same thing can occur for ionization from Ne^{2+} to Ne^{4+} and Ne^{3+} to Ne^{5+}, respectively.

In the MCDF calculations, we considered all possible configuration states and assumed that electrons distribute according to the statistical weights as initial states. Experimentally, the extracted ion beam from the ECR ion source may include core-excited ions. The fraction of the core-excited configurations can be confirmed by diagnosing the ion source plasma or the extracted beam. Another method is to compare the experimental results with calculations precisely as discussed in the previous paper for the case of the photoionization of Ne^{3+} [34]. Although for the latter case the present data were not sufficient to discuss the details of the core-excited ions, the fraction of that may be small, as was shown in our previous paper.

B. Ionization of doubly charged neon ions

Figure 3(a) shows the experimental result of photoion yield measurement from Ne^{2+} to Ne^{3+} in the energy range from 850 to 863 eV. The error is about ±12% at the maximum peak point. The spectrum is the sum of 14 scans in the same energy range.

The same calculation procedure as in the case of Ne^+ was taken for the MCDF calculations for Ne^{2+}. The total energy and higher-order correction of the initial states including $1s^22s^22p^4$ ($^3P_2$, $^3P_1$, $^3P_0$, $^1D_2$, and $^1S_0$) are summarized in Table III. The amount of energy correction for the excited level calculations is, for example, 0.706 eV for $^3P_2$.

In Table IV, the energy levels and the oscillator strengths for Ne^{2+} are shown. In the energy range, 14 configuration states are possible theoretically. In the table we only show the eight configuration states with an oscillator strength larger than 0.01. In Fig. 3(b), the theoretical line spectrum and its convolution with the system resolution are shown. Figure 3(a) shows that the peak consists of two major peaks. The MCDF calculation reproduces well these peaks. The energy position of the higher-energy side peak in Fig. 3(a) is estimated from a curve fit to be about 856.9 eV. The calculation shows good agreement with the experimental result although the calculated energy scale should be shifted by

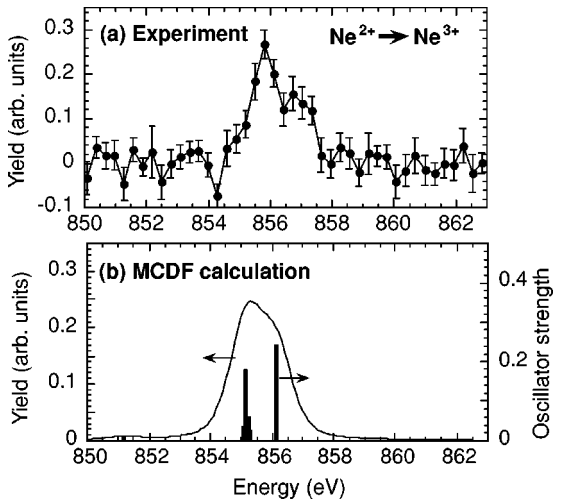

FIG. 3. (a) Relative photoion yield from Ne^{2+} to Ne^{3+} with an energy resolution of $E/\delta E \sim 670$ at the energy between 850 and 863 eV. (b) Calculated oscillator strength and convoluted spectrum with the system resolution. Statistical weights are multiplied for the calculated oscillator strength.

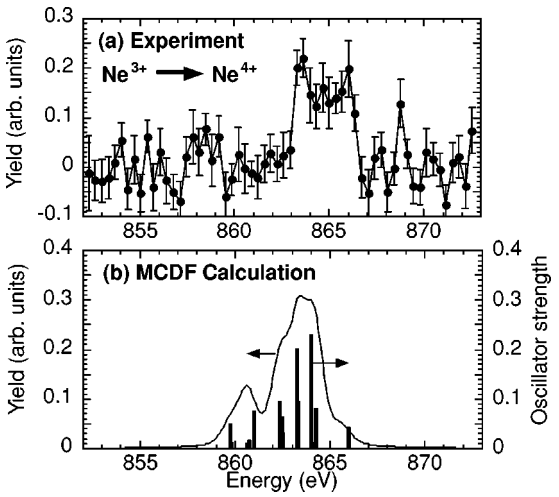

FIG. 4. (a) Relative photoion yield from Ne^{3+} to Ne^{4+} with an energy resolution of $E/\delta E \sim 770$ at the energy between 853 and 873 eV. The data of Ne^{3+} photoionization were from Ref. [28]. (b) Calculated oscillator strength and convoluted spectrum with the system resolution. Statistical weights are multiplied for the calculated oscillator strength.

about 0.6 eV to the higher-energy side. It is theoretically indicated that the observed peak is a convolution of the transitions $^3P_1 \rightarrow {}^3P_2, {}^3P_1, {}^3P_0; {}^3P_2 \rightarrow {}^3P_2, {}^3P_1; {}^3P_0 \rightarrow {}^3P_1$; and $^1D_2 \rightarrow {}^1P_1$. The most intense lines are $^3P_2 \rightarrow {}^3P_2$ and $^1D_2 \rightarrow {}^1P_1$ as shown in Table IV.

C. Ionization of triply charged neon ions

The experimental results and first calculation for the photoionization of Ne^{3+} has already been published [34]. Here we made the detail MCDF calculation again in the same manner as for the Ne^{2+} case mentioned above to compare the results systematically, and the results are shown in Fig. 4 and Tables V and VI, respectively. There were 35 configuration states which consisted of 19 intense lines with an oscillator strength larger than 0.01, as shown in Table VI. In the previous calculation, we considered the configuration state to $3p$ and five excited configurations of $1s2s2p^5$, $1s2s2p^4 3p$, $1s2s^2 2p^4$, $1s2s^2 2p^3 3p$, and $1s^2 2s2p^4$. On the other hand, in this calculation we considered the configuration to the state of $4f$ for both ground and excited states, and the higher-order corrections were taken into account. When we compare these calculations, the differences of the oscillator strength and the structure of the spectrum are small and only the energy scale is changed to the lower side. Therefore, the physical contents of the previous paper do not change. These calculations shows that (i) the contribution of the excited levels is mostly from $1s2s^2 2p^4$, (ii) the line energies decrease when including higher excited levels and considering the high-order correction factors, and (iii) each oscillator strength have a little change.

TABLE III. Initial states of $1s^2 2s^2 2p^4$, the total energy, and the higher-order energy correction for Ne^{2+}.

J	Configuration state	Total energy (eV)	Higher-order correction (eV)
2	$^3P_2$	−3442.41	0.706
1	$^3P_1$	−3442.34	0.704
0	$^3P_0$	−3442.30	0.701
2	$^1D_2$	−3438.96	0.702
0	$^1S_0$	−3434.01	0.709

D. Isonuclear series of neon ions

We combine the results of Ne^{3+} photoionization in the energy range from 851 to 875 eV [34] and the present results of Ne^+ and Ne^{2+} to study isonuclear series of Ne ions. Figure 5 shows the summarized results of photoion yield measurements of Ne^+, Ne^{2+}, and Ne^{3+} photoionization in the region of $1s$-$2p$ autoionizing resonance. We tried the photoionization experiment for Ne^{4+} ions as described before. However, no peak was observed in the energy region of

TABLE IV. Calculated energy levels and oscillator strength for Ne^{2+}. In the energy range, 14 configuration states (transitions) are possible theoretically. Here only the eight configuration states with oscillator strength larger than 0.01 are shown.

Energy (eV)	Initial state $1s^2 2s^2 2p^4$	Excited state $1s2s^2 2p^5$	Oscillator strength
851.19	$^1S_0$	$^1P_1$	0.142
855.06	$^3P_1$	$^3P_2$	0.178
855.14	$^3P_2$	$^3P_2$	0.531
855.14	$^3P_0$	$^3P_1$	0.142
855.18	$^3P_1$	$^3P_1$	0.106
855.26	$^3P_2$	$^3P_1$	0.176
855.27	$^3P_1$	$^3P_0$	0.141
856.14	$^1D_2$	$^1P_1$	0.725

TABLE V. Initial states of $1s^2 2s^2 2p^3$, the total energy, and the higher-order energy correction for Ne^{3+}.

J	Configuration state	Total energy (eV)	Higher-order correction (eV)
$\frac{3}{2}$	$^4S_{3/2}$	−3380.42	0.698
$\frac{3}{2}$	$^2D_{3/2}$	−3374.90	0.691
$\frac{5}{2}$	$^2D_{5/2}$	−3374.90	0.701
$\frac{1}{2}$	$^2P_{1/2}$	−3371.35	0.701
$\frac{3}{2}$	$^2P_{3/2}$	−3371.35	0.699

852–873 eV, although we summed up 10 scanned data sets in the same energy range. This is due to the fact that the Ne^{4+} ion-beam intensity of about 3 particle-nA was about $\frac{1}{7}$ of the Ne^{3+} beam intensity and the statistics was not enough to detect the signal (the background noise was about 800 cps).

The number of calculated lines contributes to the $1s$-$2p$ autoionizing resonance increases with the charge states, and then the observed peaks become broader, which includes many transitions, because the number of possible initial and excited states increases with the increase of the charge state. The experimental results show agreement with the theory in spite of the low spectral resolution. The peak position shifts to the higher-energy side as the charge state increases. Keski-Rahkonen observed the gaseous Ne *K* x-ray spectrum photoexcited using a chromium anode x-ray generator [42]. It is interesting to compare our results to the x-ray spectrum taken by Keski-Rahkonen because he studied inverse processes,

TABLE VI. Calculated energy levels and oscillator strength for Ne^{3+}. In the energy range, 35 configuration states (transitions) are possible theoretically. Here only the 19 configuration states with oscillator strength larger than 0.01 are shown.

Energy (eV)	Initial state $1s^2 2s^2 2p^3$	Excited state $1s2s^2 2p^4$	Oscillator strength
859.76	$^2P_{3/2}$	$^2D_{5/2}$	0.251
859.81	$^2P_{3/2}$	$^2D_{3/2}$	0.044
859.81	$^2P_{1/2}$	$^2D_{3/2}$	0.115
860.61	$^2P_{1/2}$	$^2P_{3/2}$	0.104
860.61	$^2P_{3/2}$	$^2P_{3/2}$	0.384
860.72	$^2P_{3/2}$	$^4P_{1/2}$	0.087
860.72	$^2P_{1/2}$	$^4P_{1/2}$	0.172
862.33	$^4S_{3/2}$	$^4P_{5/2}$	0.474
862.47	$^4S_{3/2}$	$^4P_{3/2}$	0.315
862.53	$^4S_{3/2}$	$^2P_{1/2}$	0.157
863.30	$^2D_{5/2}$	$^2D_{5/2}$	0.671
863.31	$^2D_{3/2}$	$^2D_{5/2}$	0.043
863.35	$^2D_{5/2}$	$^2D_{3/2}$	0.018
863.36	$^2D_{3/2}$	$^2D_{3/2}$	0.472
864.15	$^2D_{5/2}$	$^2P_{3/2}$	0.763
864.16	$^2D_{3/2}$	$^2P_{3/2}$	0.056
864.27	$^2D_{3/2}$	$^4P_{1/2}$	0.398
865.62	$^2P_{3/2}$	$^2S_{1/2}$	0.216
865.62	$^2P_{1/2}$	$^2S_{1/2}$	0.100

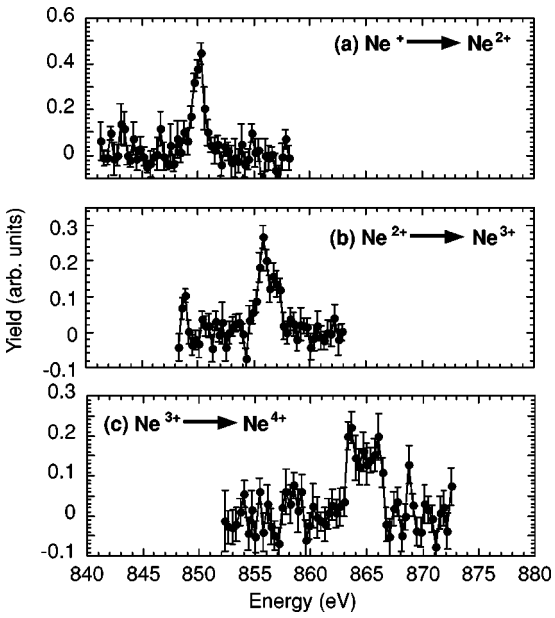

FIG. 5. Summary of relative photoion yield measurements of Ne^{2+} from Ne^+, Ne^{3+} from Ne^{2+}, and Ne^{4+} from Ne^{3+}.

although in his experiment the target was neutral gas and the number of electrons was different from our target ions. There were three separate line groups corresponding to *K*-*L*, KL-L^2, and KL^2-L^3 transitions, respectively, where the hyphen separates initial and final hole states. For example, KL-L^2 transitions start with one hole in the *K* shell and one hole in the *L* shell, and they end with two holes in the *L* shell, corresponding to our photoionization experiment of Ne^{2+} ions. Their transition energies were about 848, 854, and 862 eV, respectively. On the contrary, the center positions of each energy spectrum of photoionization are roughly 850 eV for Ne^+, 856–857 eV for Ne^{2+}, and 864–865 eV for Ne^{3+}, respectively. These values are very close to the results obtained by Keski-Rahkonen for Ne gas x-ray emissions, although the lines are shifted about 2–3 eV higher in the photoionization of neon ions. The energy differences between Ne^+ and Ne^{2+} and between Ne^{2+} and Ne^{3+} are about 6 and 8 eV, respectively. These values are almost the same as the corresponding energy differences for *K*-*L*, KL-L^2, and KL^2-L^3 transitions of neutral neons.

The energy levels of the MCDF calculations are summarized as shown in Fig. 6 for the ground states of Ne^+, Ne^{2+}, and Ne^{3+} in the region of $1s$-$2p$. It is noted that the left vertical axis is for the $1s$ level and the right axis for the $2p$ level.

IV. CONCLUSION AND PERSPECTIVE

Photoionization experiments were performed by using a merged-beam apparatus with an ECR ion source at an undulator beamline. One-electron stripped ions from Ne^+ to Ne^{2+} and from Ne^{2+} to Ne^{3+} were measured. MCDF calculations were performed to interpret the results. The isonuclear series for the photoionization of Ne^+ and Ne^{2+} are discussed with combining the results of the photoionization of Ne^{3+}. The results of MCDF calculations show good agreement with the

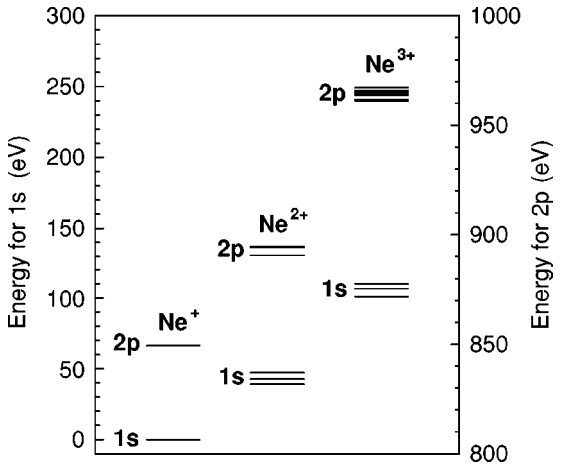

FIG. 6. Calculated energy diagram of Ne^{+}, Ne^{2+}, and Ne^{3+} in the region of $1s$-$2p$. It is noted that the left vertical axis is for the $1s$ level and the right axis for the $2p$ level.

experiments, but the fine structure of each experimental spectrum was not resolved. It may be interesting to compare the fine structure of the spectrum to understand the ionic structure precisely. It is also necessary to measure the absolute cross section with better energy resolution of the photon beam. For these reasons, the photon beam with higher flux will be desirable for a deep insight into the inner-shell physics.

These experiments represent a new step for the photoionization experiments: they allow the study of photon interaction with bound inner-shell electrons in singly and multiply charged ions, although the cross section is smaller and the experiments become difficult as the incident photon energy is going higher. If we can use He-like to Ne-like targets, the contribution to astrophysics and plasma physics will be large because they are astrophysically abundant elements. These ions will be the targets of future experiments, although the experiments for He-like or Li-like targets are more difficult due the limitations of the experimental conditions.

ACKNOWLEDGMENTS

We are grateful to Dr. T. Ishikawa of RIKEN and Dr. O. Shimomura of JAERI for giving us a chance to perform the experiments at the JAERI beamline. We thank J. Kimata of Tsukuba University, Professor T. Koizumi of Rikkyo University, Professor Y. Itoh of Josai University, Dr. T. M. Kojima of RIKEN, Professor M. Terasawa of HIT, Dr. M. Sano of JASRI, and the JAERI beamline staff of BL23SU for their help with the experiments and for their encouragement. The authors (H. Y. and M. O.) are also grateful to Dr. S. Shin of RIKEN for his understanding of and encouragement with the experiments. The experiments were performed at the SPring-8 with the approval of the Japan Synchrotron Radiation Research Institute (JASRI) under proposal numbers 2000A0189-NS-np, 2000A0099-NS-np, and 1999B0037-CS-np.

[1] K. Kawashima and S. Kitamoto, Publ. Astron. Soc. Jpn. **48**, L113 (1996).
[2] D. A. Liedahl and F. Paerels, Astrophys. J. Lett. **468**, L33 (1996).
[3] *The Opacity Project 1995* (The Institute of Physics, Bristol, 1995), Vol. 1.
[4] S. N. Nahar and A. K. Pradhan, Phys. Rev. A **49**, 1816 (1994).
[5] D. G. Hummer, K. A. Berrington, W. Eissner, A. K. Pradhan, H. E. Saraph, and J. A. Tully, Astron. Astrophys. **279**, 298 (1993).
[6] T. B. Lucatorto and T. J. McIlrath, Phys. Rev. Lett. **37**, 428 (1977).
[7] T. B. Lucatorto, T. J. McIlrath, J. Sugar, and S. M. Youngeret, Phys. Rev. Lett. **47**, 1124 (1981).
[8] I. C. Lyon, B. Peart, J. B. West, and K. Dolder, J. Phys. B **19**, 4137 (1986).
[9] I. C. Lyon, B. Peart, K. Dolder, and J. B. West, J. Phys. B **20**, 1471 (1987).
[10] I. C. Lyon, B. Peart, and K. Dolder, J. Phys. B **20**, 1925 (1987).
[11] B. Peart, I. C. Lyon, and K. Dolder, J. Phys. B **20**, 5403 (1987).
[12] B. Peart and I. C. Lyon, J. Phys. B **20**, L673 (1987).
[13] H. Kjeldsen, F. Folkmann, H. Knudsen, M. S. Rasmussen, J. B. West, and T. Andersen, J. Phys. B **32**, 4457 (1999).
[14] H. Kjeldsen, F. Folkmann, J. E. Hansen, H. Knudsen, M. S. Rasmussen, J. B. West, and T. Andersen, Astrophys. J. Lett. **524**, L143 (1999).
[15] J. B. West, T. Andersen, R. L. Brooks, F. Folkmann, H. Kjeldsen, and H. Knudsen, Phys. Rev. A **63**, 052719 (2001).
[16] T. Andersen, P. Andersen, F. Folkmann, V. K. Ivanov, H. Kjeldsen, and J. B. West, J. Phys. B **34**, 2009 (2001).
[17] J.-M. Bizau, D. Cubaynes, M. Richter, F. J. Wuileumier, J. Obert, J. C. Putaux, T. J. Morgan, E. Kallbe, S. Sorensen, and A. Damany, Phys. Rev. Lett. **67**, 576 (1991).
[18] S. Al Moussalami, J.-M. Bizau, B. Rouvellou, D. Cubaynes, L. Journel, F. J. Wuileumier, J. Obert, J. C. Putaux, T. J. Morgan, and M. Richter, Phys. Rev. Lett. **76**, 4496 (1996).
[19] J.-M. Bizau, J.-M. Esteva, D. Cubaynes, F. J. Wuileumier, C. Blancard, A. Compant La Fontaine, C. Couillaud, J. Lachkar, R. Marmoret, C. Rémond, J. Bruneau, D. Hitz, P. Ludwig, and M. Delaunay, Phys. Rev. Lett. **84**, 435 (2000).
[20] E. Jannitti, M. Gaye, M. Mazzoni, P. Nicolosi, and P. Villoresi, Phys. Rev. A **47**, 4033 (1993).
[21] G. O'Sullivan, C. McGuinness, J. T. Costello, E. T. Kennedy, and B. Weinmann, Phys. Rev. A **53**, 3211 (1996).
[22] T. Koizumi, Y. Itoh, M. Sano, M. Kimura, T. M. Kojima, S. Kravis, A. Matsumoto, M. Oura, T. Sekioka, and Y. Awaya, J. Phys. B **28**, 609 (1995).
[23] Y. Itoh, T. Koizumi, Y. Awaya, S. D. Kravis, M. Oura, M. Sano, T. Sekioka, and F. Koike, J. Phys. B **28**, 4733 (1995).
[24] T. Koizumi, Y. Awaya, M. Gonno, Y. Itoh, M. Kimura, T. M. Kojima, S. Kravis, M. Oura, M. Sano, T. Sekioka, N. Watanabe, H. Yamaoka, and F. Koike, J. Electron Spectrosc. Relat. Phenom. **79**, 289 (1996).

[25] M. Sano, Y. Itoh, T. Koizumi, T. M. Kojima, S. D. Kravis, M. Oura, T. Sekioka, N. Watanabe, Y. Awaya, and F. Koike, J. Phys. B **29**, 5305 (1996).
[26] T. Koizumi, Y. Awaya, A. Fujino, Y. Itoh, M. Kitajima, T. M. Kojima, M. Oura, R. Okuma, M. Sano, T. Sekioka, N. Watanabe, and F. Koike, Phys. Scr. **T73**, 131 (1997).
[27] T. M. Kojima, M. Oura, Y. Ito, T. Koizumi, M. Sano, T. Sekioka, N. Watanabe, H. Yamaoka, and Y. Awaya, J. Phys. B **31**, 1463 (1998).
[28] N. Watanabe, Y. Awaya, A. Fujino, Y. Itoh, M. Kitajima, T. M. Kojima, M. Oura, R. Okuma, M. Sano, T. Sekioka, and T. Koizumi, J. Phys. B **29**, 4137 (1998).
[29] Y. Itoh, A. Ito, M. Kitajima, T. Koizumi, T. M. Kojima, H. Sakai, M. Sano, and N. Watanabe, J. Phys. B **34**, 3493 (2001).
[30] I. P. Grant, B. J. McKenzie, P. H. Norrington, D. F. Mayers, and N. C. Pyper, Comput. Phys. Commun. **21**, 207 (1980).
[31] F. A. Parpia, I. P. Grant, and C. F. Fischer (private communication); K. G. Dyall, I. P. Grant, C. T. Johnson, F. A. Parpia, and E. P. Plummer, Comput. Phys. Commun. **55**, 425 (1989).
[32] X. M. Tong and S. Chu, Phys. Rev. A **55**, 3406 (1997).
[33] X. M. Tong, D. Kato, T. Watanabe, and S. Ohtani, J. Phys. B **33**, 717 (2000).
[34] M. Oura, H. Yamaoka, K. Kawatsura, J. Kimata, T. Hayaishi, T. Takahashi, T. Koizumi, T. Sekioka, M. Terasawa, Y. Itoh, Y. Awaya, A. Yokoya, A. Agui, A. Yoshigoe, and Y. Saitoh, Phys. Rev. A **63**, 014704 (2001).
[35] M. Oura, T. M. Kojima, Y. Awaya, Y. Itoh, K. Kawatsura, M. Kimura, T. Koizumi, T. Sekioka, H. Yamaoka, and M. Cox, J. Synchrotron Radiat. **5**, 1058 (1998).
[36] M. Oura, H. Yamaoka, K. Kawatsura, T. Hayaishi, J. Kimata, T. M. Kojima, M. Kimura, T. Sekioka, and M. Terasawa, Rev. Sci. Instrum. **71**, 1206 (2000).
[37] B. L. Henke, J. P. Knauer, and K. Premaratne, J. Appl. Phys. **52**, 1509 (1981).
[38] A. Yokoya, T. Sekiguchi, Y. Saitoh, T. Okane, T. Nakatani, T. Shimada, H. Kobayashi, M. Takao, Y. Teraoka, Y. Hayashi, S. Sasaki, Y. Miyahara, T. Harami, and T. A. Sasaki, J. Synchrotron Radiat. **5**, 10 (1998).
[39] S. Sasaki, Nucl. Instrum. Methods Phys. Res. A **347**, 83 (1994).
[40] V. Schmidt, *Electron Spectroscopy of Atoms Using Synchrotron Radiation* (Cambridge University Press, Cambridge, 1997), p. 58.
[41] U. Arp, K. Iemura, G. Kutluk, T. Nagata, S. Yagi, and A. Yagishita, J. Phys. B **32**, 1295 (1999).
[42] O. Keski-Rahkonen, Phys. Scr. **7**, 173 (1973).